Computer Modeling in
Engineering & Sciences

Tech Science Press

https://doi.org/10.32604/cmes.2026.078932

ARTICLE

Structural Integrity of GFRP Absorption Towers under Lifting Loads: Design and FEA Validation of a Bolt-On Steel Reinforcement System

Matías Mariqueo[1,2], Rodrigo Valle[3], César Garrido[4], Sebastián Andrés Toro[5] and Víctor Tuninetti[1,*]

[1]Department of Mechanical Engineering, Universidad de La Frontera, Temuco, Chile
[2]Mechanical Engineering Program, Universidad de La Frontera, Temuco, Chile
[3]Construction Multidisciplinary Research Group, Facultad de Arquitectura, Construcción y Medio Ambiente, Universidad Autónoma de Chile, Talca, Chile
[4]Department of Mechanical Engineering, Universidad del Bío-Bío, Concepción, Chile
[5]Departamento de Ingeniería Mecánica, Universidad de Santiago de Chile, USACH, Av. Bernardo O'Higgins 3363, Santiago, Chile

*Corresponding Author: Víctor Tuninetti. Email: victor.tuninetti@ufrontera.cl

Received: 10 January 2026; Accepted: 23 February 2026; Published: 28 August 2026

ABSTRACT: Lifting and maintenance of existing Glass-Fiber Reinforced Polymer (GFRP) absorption towers pose significant structural risks, as these units were often not designed for such loads. Previous research has established that lifting these sections without reinforcement results in critically low factors of safety (1.9–2.5) due to high stress concentrations on the composite flanges. This paper presents the design, analysis, and validation of a novel bolt-on steel lifting system to mitigate these structural risks. A system comprising a 32 mm thick ASME A36 steel blind flange with integrated lifting lugs and half-moon stiffeners was designed to mount to the tower's existing bolt pattern. Using Finite Element Analysis (FEA) with the Hashin failure criterion, the full assembly of steel elements and GFRP tower section was simulated under vertical, horizontal, and complex transition-al-angle lifting scenarios. The new lifting system substantially improves structural integrity. The design effectively transfers stresses from the fragile GFRP flange to the robust steel elements, resulting in a 31% reduction in maximum stresses on the GFRP shell during vertical lifts and a 35% reduction during horizontal lifts. Consequently, the minimum safety factor for the GFRP tower increased from 1.9 to 3.8 in the horizontal case and from 4.1 to 11.7 in the vertical case, representing an average safety factor increase of 286%. The steel components themselves were validated with safety factors exceeding 5, compliant with lifting standards. This paper provides a validated engineering blueprint for a bolt-on system that ensures the safe and reliable lifting of GFRP composite towers. This design successfully resolves the critical safety flaws identified in our previous analysis.

KEYWORDS: Glass-fiber reinforced polymer (GFRP); composite structures; finite element analysis (FEA); lifting operations; structural integrity; below-the-hook; mitigation strategy

1 Introduction

Glass-Fiber Reinforced Polymer (GFRP) composites have been progressively adopted in industrial applications where corrosion resistance and long-term durability are critical performance requirements [1–3]. Preliminary industrial studies demonstrated that GFRP components outperform their metal counterparts in aggressive chemical environments, particularly in pulp and paper mills, where exposure to acidic and humid conditions accelerates steel degradation [4,5]. Later applications confirmed that GFRP enables the construction of large-scale equipment, such as gas absorption towers and scrubbers, while maintaining low structural weight and favorable installation logistics [6,7]. Comparative evaluations between composite and metal vessels further highlighted the economic and operational advantages of GFRP under long-term service conditions [8,9].

Subsequent research focused on the structural efficiency of GFRP towers, confirming reliable performance in service over extended operating periods, reinforcing the suitability of GFRP for vertical process equipment [10]. However, these same studies revealed a critical limitation: most existing GFRP towers were designed exclusively for operational loads, without considering dismantling, relocation, or major maintenance interventions during their service life [11,12]. Similarly, research on the life cycle of composite structures has shown that this lack of foresight often leads to the premature decommissioning of assets that would otherwise be structurally reliable [13]. Research on aged composites has shown that, while laminate degradation is typically minimal, extraordinary loading situations associated with maintenance activities can lead to structural failure [14,15]. Lifting operations required for inspection, renovation, or plant reconfiguration introduce load combinations that differ fundamentally from design service conditions [16]. Therefore, design frameworks for durability emphasize the importance of considering these non-operational loading scenarios when evaluating the remaining service life of composite structures [17].

Nevertheless, the structural risks associated with lifting are particularly pronounced in large vertical GFRP towers, where the available lifting points are often limited to existing flanged connections [18,19]. Studies on the handling of composite vessels have shown that lifting loads generate combined axial, bending, and shear stresses that are not adequately captured by conventional design approaches [20,21]. Advanced numerical investigations further demonstrated that these loading conditions can trigger localized overstressing even when overall stress levels remain moderate [22,23]. The deficiency of GFRP structures under lifting conditions is mainly concentrated in bolted flange connections. Fundamental research on composite joints has established that the anisotropic and layered nature of GFRP produces highly non-uniform stress distributions around bolt holes [24]. This behavior is markedly different from that of isotropic metal joints and becomes more critical in filament-wound structures, where layer orientation determines load transfer mechanisms [25]. Several authors have reported that localized stress concentrations at GFRP joints can lead to brittle failure mechanisms, including fiber breakage and matrix cracking, which often occur without significant prior deformation [26]. To model this behavior, Hashin-type failure criteria have been widely adopted and validated to predict the onset of damage in composite laminates subjected to complex stress states [27–29]. Further numerical studies extended these criteria to capture the progressive evolution of damage, allowing for more realistic predictions of stiffness degradation and failure propagation in bolted composite joints [30].

Research into damage mechanics revealed that cracking of the matrix often precedes more severe modes of damage, such as delamination and fiber breakage [31]. Experimental observations confirmed that cracking at the layer level acts as a trigger for damage through the thickness. Therefore, progressive damage modeling approaches that incorporate these mechanisms have become essential tools for assessing the structural integrity of composite connections [32]. The geometric discontinuities introduced by bolt holes have been identified as a source of stress concentration in composite flanges. Prior work indicates that circular bolt holes significantly amplify local stresses, especially when the distances to the edges and the spacing between bolts are limited [33]. Alternative hole geometries and reinforcement strategies have been proposed to mitigate these effects, showing partial reductions in stress concentration at the laminate level [34,35]. Additionally, recent work by Li et al. [36] systematically evaluated techniques such as adhesive filling and elliptical perforations, demonstrating that these micro-level modifications can significantly improve the bearing capacity of GFRP bolted connections. However, subsequent research indicated that these approaches may be insufficient for large-scale industrial components subjected to high lifting loads [37]. Similarly, manufacturing imperfections further complicate the performance of GFRP bolted joints. Studies on filament-wound structures indicate that variability in fiber volume fraction, resin concentration zones, and local misalignment can significantly reduce joint strength compared to idealized numerical models [38]. Additional research explored the influence of bolt preload and joint geometry on local crushing and bearing failure in composite flanges. These studies demonstrated that even optimized bolt arrangements cannot completely eliminate localized damage under high transverse loads [39]. Progressive damage simulations confirmed that local crushing and shear failure remain critical modes in joints subjected to high loads [40,41].

Numerical investigations have demonstrated the effectiveness of finite element analysis (FEA) for evaluating stresses induced by lifting in large composite structures [42]. However, most existing studies focus on generic composite plates or simplified joints, rather than full-scale industrial geometries [43]. As a result, validated engineering solutions for handling actual composite vessels remain in their infancy [44]. In this context, our previous research [4] established a comprehensive finite element baseline for lifting-induced stresses in full-scale GFRP absorption towers. That study demonstrated that lifting tower sections using their original bolted flanges leads to severe stress concentrations at bolt holes and critically low safety factors, proving such operations to be structurally unsafe without reinforcement. These findings align with established principles for lifting accessories, which emphasize the need for dedicated load transfer components for non-standard lifting operations [45].

Various approaches have been explored to reinforce metal or composite flanges and structural elements, such as external clamping rings, reinforcement collars, and locally bonded reinforcements. Adhesively bonded reinforcements and externally bonded FRP systems have been widely utilized to improve the structural capacity of existing components by enhancing local load distribution and mitigating stress concentrations [46,47]. However, these methods typically require exhaustive surface preparation and the maintenance of a high-quality adhesive bond, both of which are highly sensitive to environmental conditions and require rigorous installation procedures that are often impractical in field-maintenance scenarios [46]. In contrast, the present study proposes a fully bolted lifting system specifically engineered for field application on existing GFRP towers. Unlike traditional reinforcement collars or bonded patches, this system functions as a macro-level mechanical retrofit that utilizes the tower's existing bolt pattern. The proposed configuration does not require permanent alterations to the composite laminate or chemical surface adhesion, making it a fully reversible solution that is independent of surface quality and environmental constraints. This approach effectively bridges the gap between micro-level joint modification and heavy industrial clamping systems, providing a field-ready blueprint for the safe handling of large-scale composite assets.

Thus, despite the extensive literature on the behavior of composite joints, damage modeling and hoisting analysis represent a gap in research [46–49]. There are no reports of field-applicable engineering solutions for GFRP absorption tower flanges that can safely support lifting operations, particularly in scenarios involving combined vertical, horizontal, and transition angle loads. Existing studies focus on material-scale improvements, the optimization of isolated joints, or numerical methodologies, without providing a practical modernization strategy compatible with industrial constraints [50–52]. Therefore, to address this gap, this paper proposes and validates a novel bolt-on steel lifting system, specifically designed for the lifting of existing GFRP absorption towers. The system functions as a non-invasive retrofit that transfers lifting loads from vulnerable composite flanges to robust steel components. Through detailed finite element analysis, the performance of the proposed system is evaluated under vertical, horizontal, and transition angle lifting conditions. The resulting localized stresses and improvements in structural safety factors are quantified, providing a validated model for the safe maintenance and handling of GFRP composite towers [53–56].

2 Materials and Methods

2.1 Design of the Bolt-On Lifting System

Based on the demonstrated need for a mitigation strategy [1], a bolt-on steel hoisting system was designed. This system consists of two primary components (Fig. 1), a 32 mm thick blind flange with two integrated lifting lugs, and two half-moon stiffeners that bolt to the underside of the tower's flange. All components were designed using ASME A36 steel, selected for its wide availability and well-defined mechanical properties (Yield Strength: 250 MPa; Young's Modulus: 200 GPa). The 32 mm flange thickness was selected based on preliminary sensitivity FEA to minimize deflection and rigidify the GFRP flange using five configurations (Fig. 2). The lifting lugs were designed according to industry guidelines and joined to the flange via Shielded Metal Arc Welding (SMAW) with an E7015 electrode, per AWS D1.1 standards. The entire system was designed to attach to the tower's existing 48-hole bolt pattern using 5/8″ ASME A307 bolts.

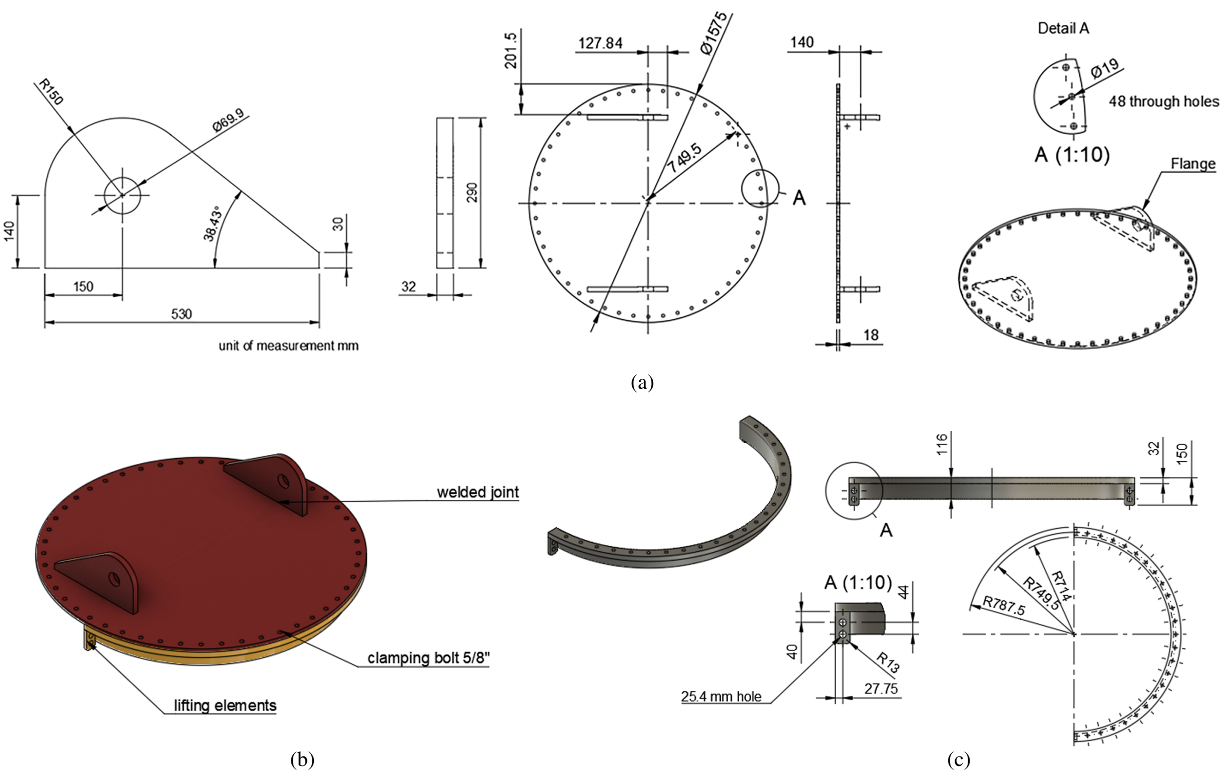

Figure 1: Schematics of the bolt-on steel lifting system: (**a**) Technical drawings and dimensions of the 32 mm thick ASME A36 blind flange with integrated lifting lugs. (**b**) 3D isometric view of the complete assembly showing the blind flange, 5/8″ clamping bolts, and the lifting elements (stiffeners) positioned on the GFRP flange. (**c**) Detailed dimensions of the half-moon stiffener used to reinforce the underside of the GFRP flange.

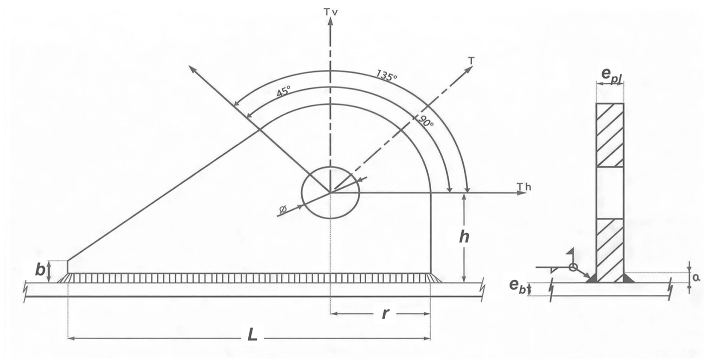

Blind Flange Thickness (e_b) [mm]	Lifting Lug Thickness (e_{pl}) [mm]	Shackle Hole Diameter [mm]	*h* [mm]	*b* [mm]	*L* [mm]	*r* [mm]
18	18	35.1	70	20	240	70
22	22	41.1	80	20	290	80
28	28	50.8	90	20	350	90
30	30	57.2	110	30	400	120
32	32	69.9	140	30	530	150

Figure 2: Five levels configurations of the blind flange thickness (e_b): 18, 22, 28, 30, and 32 mm for sensitivity analysis and design optimization.

2.2 Finite Element Model (FEM) Configuration

The structural analysis was performed using ANSYS Workbench, employing the Mechanical and Composite Pre/Post (ACP) modules. The GFRP tower sections were modeled as surface geometries to accurately capture laminate behavior, a method validated in our previous work [1], while the new steel lifting system components were modeled as 3D solids and integrated into the assembly. The GFRP laminate was defined in ACP (Pre) based on technical drawings, consisting of a MWM (Mat, Woven Roving, Mat) sequence with fibers modeled at a ±55° angulation relative to the tower's Y-axis. The laminate sequence for the main 14 mm shell (5 MWM) was [Mat at 55°, Woven Roving at −55°, Mat at 55°, Mat at −55°, Woven Roving at 55°, Mat at −55°], with thicknesses of [0.8/1.0/0.8/0.8/1.0/0.8 mm], respectively. The ±55° fiber orientation adopted in the GFRP laminate is based on standard filament winding practice for cylindrical composite structures. This specific stack-up is commonly employed because it provides an efficient balance between axial, circumferential, and in-plane shear stiffness, allowing the laminate to withstand complex multiaxial stress states [57]. Under lifting conditions, the tower experiences a combination of axial loads, bending moments, and shear forces, especially during the horizontal and transition lifting configurations. The ±55° orientation is ideally suited to these anticipated load paths, as it facilitates the effective redistribution of stress within the laminate and avoids structural dependence on a single dominant fiber direction [58]. This ensures the structural integrity of the shell mantle when subjected to the concentrated forces transmitted by the bolted steel reinforcement system.

Orthotropic properties for the GFRP layers (sourced from the ASME RTP-1 standard) and isotropic properties for the ASME A36 steel are detailed in Table 1. A face mesh with sizing controls was applied to the GFRP surfaces, with finer refinement in critical zones (bolt holes, fillets) based on the prior convergence study [1]. The GFRP shell was meshed using SHELL181 elements, with a typical section consisting of approximately 78,400 nodes and 76,500 elements. Due to the scale of the assembly and the high number of fasteners, the 48 bolts were not modeled explicitly with frictional contacts. Instead, bonded contact definitions were employed between the steel and GFRP flange faces. This simplification is supported by the work of Tanlak et al. [59], who demonstrated that simplified finite element models for bolted joints provide a reliable prediction of the assembly's global stiffness and deformation behavior while significantly reducing computational cost compared to detailed 3D solid models. The bonded condition simulates a no-slip state, assuming sufficient bolt preload is applied to maintain joint integrity during the lift. This approach effectively captures the macroscopic load transfer required for the tower's structural assessment, while the bolts themselves were verified analytically to ensure safety (Section 3.4). Consequently, since the bonded formulation mathematically enforces kinematic continuity (preventing relative sliding), the coefficient of friction was not an active parameter in the simulation. The normal contact stiffness was defined by the solver using a program-controlled penalty formulation based on the material moduli of the mating surfaces, ensuring a rigid load transfer consistent with the no-slip design assumption. Due to element count limitations, the 48 bolts were not modeled explicitly; instead, bonded contact definitions were used between the steel and GFRP flange faces to simulate a rigid, bolted connection.

Table 1: Mechanical properties of materials used in the Finite Element Analysis.

Property	Direction	Units	GFRP Woven Roving	GFRP Mat	ASME A36 Steel
Density	–	kg/m^3	1850	1508.6	7850
Young's Modulus	X	MPa	24,355	7069	200,000
	Y	MPa	24,355	7069	200,000
	Z	MPa	5154.6	5268	200,000
Poisson's Ratio	xy	–	0.3011	0.3269	0.26
	yz	–	0.28	0.28	0.26
	xz	–	0.28	0.28	0.26
Shear Modulus	xy	MPa	1895	2663	79,300
	yz	MPa	1532	2152	79,300
	xz	MPa	1532	2152	79,300
Yield Strength	–	MPa	N/A	–	250
Tensile Strength (GFRP)	X	MPa	487.1	106.03	–
Compressive Strength (GFRP)	X	MPa	−292.3	−141.3	–

The numerical reliability of the finite element model was verified through a mesh convergence study previously performed using the same formulation, material properties, and loading conditions [4]. Systematic mesh refinement in critical regions, particularly around the flange geometry and bolt holes, resulted in variations of less than approximately 5% in the maximum equivalent stress values. This level of convergence confirms that the results presented in this study are mesh-independent, ensuring a robust balance between computational efficiency and the precision required to evaluate the structural integrity of the reinforced tower sections.

2.3 Load Cases and Boundary Conditions

The analysis validated the full system (GFRP tower + steel elements) under three scenarios, as illustrated in Fig. 3. All simulations included standard earth gravity and a static 50,000 N (5000 kg) load representing the ceramic packing, applied at the tower's internal support ring. The first scenario was a Vertical Lift (Case 1), where a Fixed Support boundary condition was applied to the holes of the lifting lugs on the top blind flange. The second scenario, a Horizontal Lift (Case 2), applied Fixed Supports to the lugs on both the top and bottom blind flanges, with the packing load distributed over the most critical 12.5% of the inner shell [1].

Finally, Transitional Lifts (Case 3) were analyzed by simulating the horizontal lift model at inclinations of 67.5°, 45°, and 22.5°. For failure analysis, the von Mises stress criterion was used to evaluate the isotropic steel components (ASME A36), while the Hashin failure criterion was used to evaluate the orthotropic GFRP laminates.

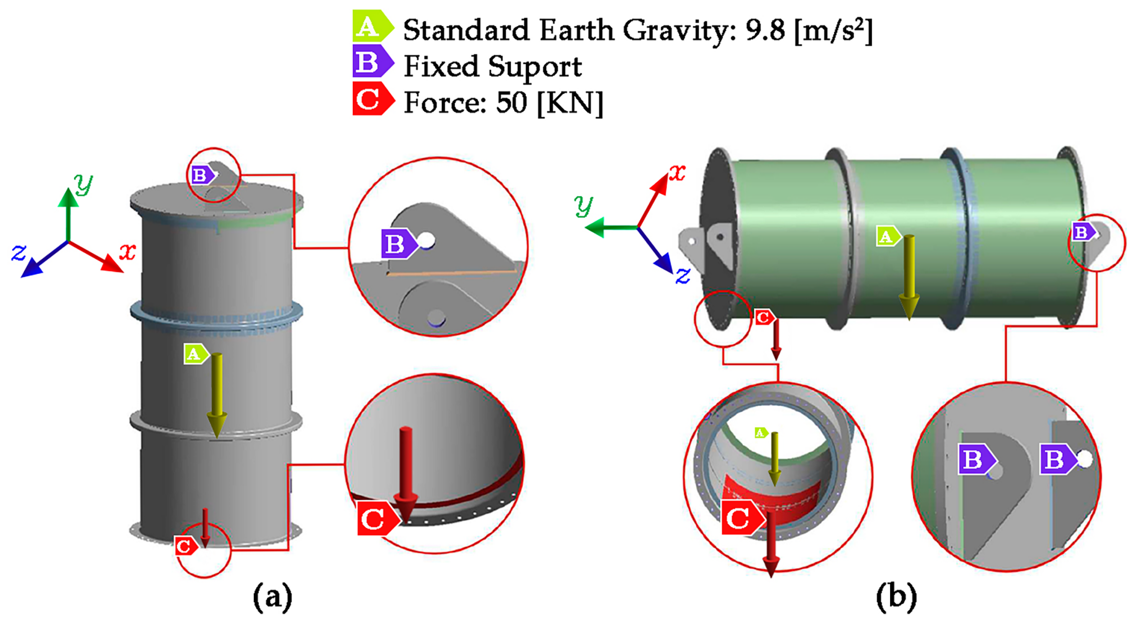

Figure 3: FEA Model and Load Cases. (**a**) Vertical lift model showing fixed support on top lugs and internal packing load. (**b**) Horizontal lift model showing fixed supports on lugs at both ends.

In the numerical model, the ceramic packing was represented as a static load applied to the inner support ring, assuming a nominally centered center of gravity. In practical lifting operations, deviations from this ideal condition may occur due to non-uniform distribution of the packing, installation tolerances, or partial removal of the packing, resulting in load eccentricity and additional bending effects. Thus, a displaced center of gravity would mainly increase the bending moments and the asymmetric distribution of stress in the tower shell. It should be noted that the horizontal and transition hoisting configurations analyzed in this study introduce asymmetric load paths and high bending demands, which partially neutralize the effects associated with packing load eccentricity. Therefore, the proposed bolt-on hoisting system demonstrates robustness against actual variations in packing load distribution.

3 Results

The structural integrity of the proposed lifting system was evaluated by analyzing the stress distributions and factors of safety (FoS) for both the steel components and the GFRP composite sections under three distinct loading scenarios.

3.1 Design Optimization and Sensitivity Analysis

To ensure the engineering guiding value of this research, the FEA model was initially utilized as an optimization tool to determine the critical dimensions of the steel reinforcement system. A sensitivity analysis was conducted on the blind flange thickness (e_b), evaluating five levels: 18, 22, 28, 30, and 32 mm. To rigorously identify the optimal design point, these configurations were subjected to a design verification load of 70,000 N. This load exceeds the standard 50,000 N operational load by 40% to simulate extreme handling impacts and ensure a robust safety margin during field implementation.

The structural response proved highly sensitive to thickness variations (Table 2). At e_b = 18 mm, the system experienced mechanical failure with a maximum equivalent stress above elastic limit (for pure elastic model: 714.8 MPa and 19.63 mm displacement, FoS of 0.35). The comparative stress contours (Fig. 4) show the 18 mm configuration fails to adequately rigidify the connection, leading to failure.

Table 2: Optimization data for the steel blind flange thickness (e_b) under a 70 kN verification load.

Flange Thickness (e_b) [mm]	Max. Displacement [mm]	Max. Stress [MPa]	Min. FoS (Steel Yield)
18	19.63	714.8	0.35
22	10.4	435.2	0.57
28	4.91	249.7	0.99
30	3.63	197.3	1.26
32 (Selected Design)	2.6	153.6	1.62

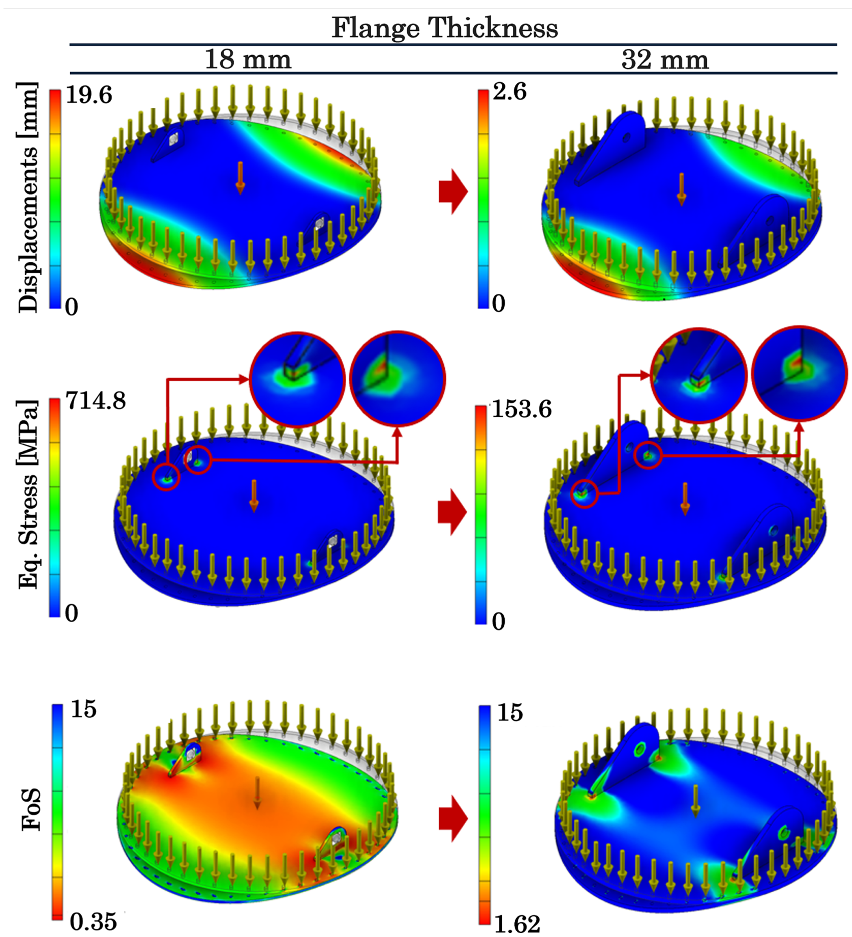

Figure 4: Comparative FEA stress contours for the 18 mm (preliminary design) vs. 32 mm (optimized design) configurations under a 70,000 N verification load showing transition from a failure state to a structurally stable regime.

In contrast, the 32 mm thickness was validated as the optimal design point, as it effectively rigidified the assembly, reducing stress to 153.6 MPa and ensuring a stable FoS of 1.62 under the extreme verification load. This optimized geometry was subsequently used for all operational lifting scenarios (Sections 3.2–3.4).

3.2 Performance during Vertical Lift

Fig. 5 presents the stress contours for the critical tower segment 2 during the vertical lift. The steel blind flange and lifting lugs exhibited robust performance, effectively transferring the tensile loads. As shown in Fig. 5a, the maximum von Mises stress of 79.35 MPa was localized at the weld toe connecting the lifting lug to the flange plate. This stress concentration dissipates rapidly into the surrounding plate, and the component maintains a minimum FoS of 5.04 against the yield strength of ASME A36 steel (250 MPa), satisfying the safety requirements. The analysis of the composite structure (Fig. 5b) confirms that the steel system effectively distributes the vertical tension load preventing localized damage. The maximum equivalent stress on the GFRP shell was negligible, peaking at 2.13 MPa in the upper mantle zone of tower segment 2. The Hashin failure criterion indicated a minimum FoS of 11.2, confirming that the composite operates well within its elastic limit during vertical hoisting.

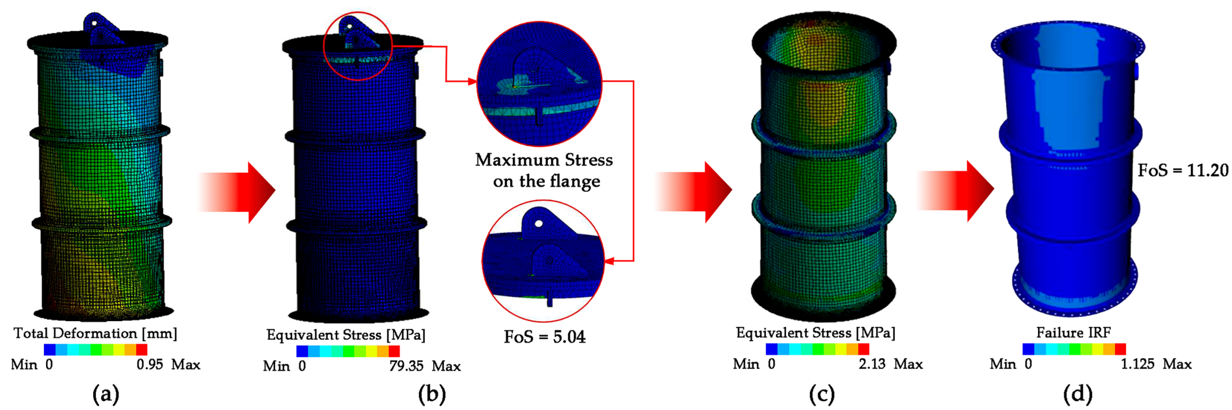

Figure 5: Vertical lift results of the complete system in tower segment 2. (**a**) Distribution of equivalent deformations of the complete system. (**b**) Distribution of equivalent stresses of the complete system. (**c**) Distribution of stresses in the GFRP tower section. (**d**) Distribution of the Hashin failure index (HFI) in the GFRP laminate.

3.3 Performance during Horizontal and Transitional Lifts

The horizontal lift introduces significant bending moments due to the cantilevered weight of the ceramic packing. Fig. 6 illustrates the results for the most critical horizontal case (Section 1 with distributed packing load). The steel components effectively absorbed the bending stresses, registering a maximum von Mises stress of 39.08 MPa at the lug-flange interface, corresponding to a high FoS of 7.6. The composite shell (Fig. 6b) exhibited a maximum stress of 5.68 MPa located at the mantle near the lower structural reinforcement band. Despite this increase compared to the vertical case, the minimum FoS remained at 3.8, confirming structural stability. To capture non-linear load effects during the lifting maneuver, the transition from horizontal to vertical was analyzed at inclination angles of 67.5°, 45°, and 22.5°. The results indicated a non-linear relationship between inclination and stress. The GFRP shell stress was lowest at the 67.5° inclination (1.65 MPa, FoS 14.3) and remained stable at 45° (1.70 MPa, FoS 13.2). As the gravity vector shifted at the 22.5° inclination, stresses increased to 4.73 MPa (FoS 5.2), approaching the horizontal values. Throughout the entire transition, the steel components maintained an FoS above 7.6, proving the system is safe throughout the complete dynamic lifting motion.

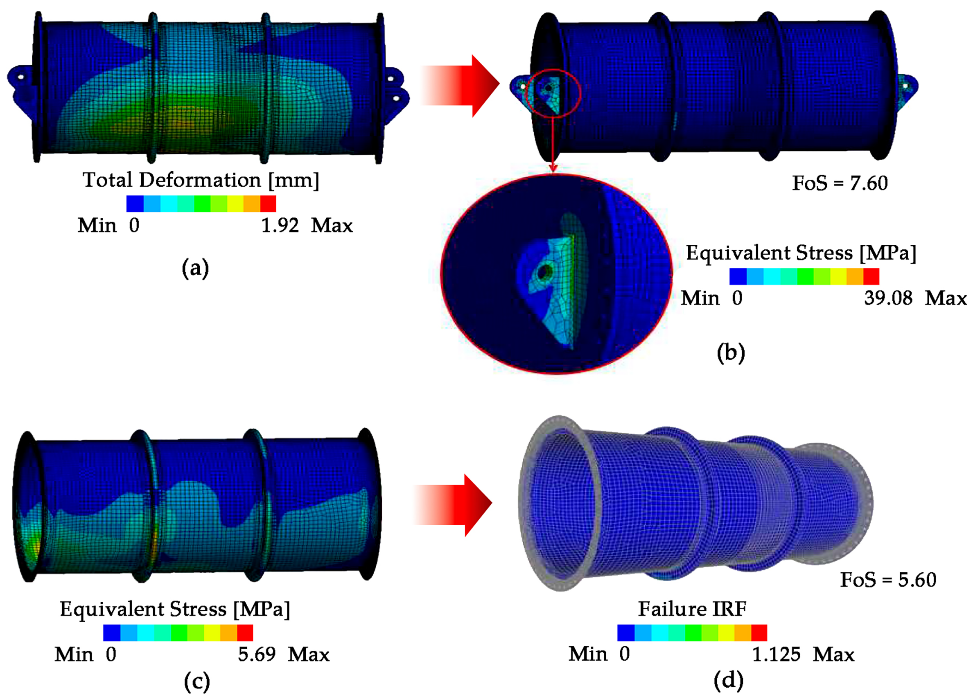

Figure 6: Results of horizontal lifting of the complete system in Section 1 (most critical case). (**a**) Distribution of equivalent deformations of the complete system. (**b**) Distribution of equivalent stresses of the complete system. (**c**) Distribution of stresses in the GFRP tower section. (**d**) Distribution of the Hashin failure index (HFI) in the GFRP laminate.

The reported values demonstrate a non-linear relationship between the elevation inclination (θ) and the structural response of the GFRP shell. As the tower moves from a vertical (90°) to a horizontal (0°) orientation, the structural demand increases non-monotonically due to the trigonometric decomposition of the gravitational load into axial ($F_y = Fsin\theta$) and transverse ($F_x = Fcos\theta$) components [4]. To further clarify this effect, Table 3 summarizes the maximum equivalent stress and the corresponding minimum FoS obtained for the vertical, transitional, and horizontal lifting configurations using the selected 32 mm design. The data reveals a pronounced non-linear escalation in stress as the angle drops below 45°, where bending moments at the flange interface become the primary driver of the stress state. Despite this increased demand, the reinforcement system ensures that the FoS remains above 3.8, confirming that the GFRP remains well within the linear elastic regime throughout the entire maintenance maneuver.

Table 3: Non-linear evolution of structural response of the GFRP shell as a function of the inclination angle (θ).

Inclination Angle (θ, °)	Max GFRP Stress (MPa)	Minimum FoS
90 (Vertical)	2.13	11.2
67.5	1.65	14.3
45.0	1.70	13.2
22.5	4.73	5.2
0 (Horizontal)	5.68	3.8

3.4 Core Finding: Direct Comparison and Mitigation

The efficacy of the proposed design is quantified by comparing these results against the baseline preliminary study (lifting without the steel system) [1]. The steel flange system successfully rigidified the connection points, preventing the localized deformation of the GFRP observed in the baseline study. As detailed in Fig. 7, maximum stresses on the GFRP shell were reduced by 31% (from 4.77 to 3.26 MPa) during the vertical lift and reduced by 35% (from 8.74 to 5.68 MPa) during the critical horizontal lift. This stress reduction resulted in a substantial improvement in the safety margin, as shown in Fig. 8. The minimum FoS for the vertical lift increased from a baseline of 4.1 to 11.7 (a 286% improvement). Crucially, for the horizontal lift, the minimum FoS was raised from a critical 1.9 to a safe 3.8, effectively mitigating the risk of failure. Finally, the analytical verification of the 5/8″ ASME A307 connecting bolts confirmed they are not a weak point in the assembly, exhibiting safety factors of 46.9 in tension and 40.5 in shear. The analysis validated the performance of the new bolt-on steel hoisting system by evaluating the stresses on both the steel components using the von Mises criterion and the GFRP tower using the Hashin criterion.

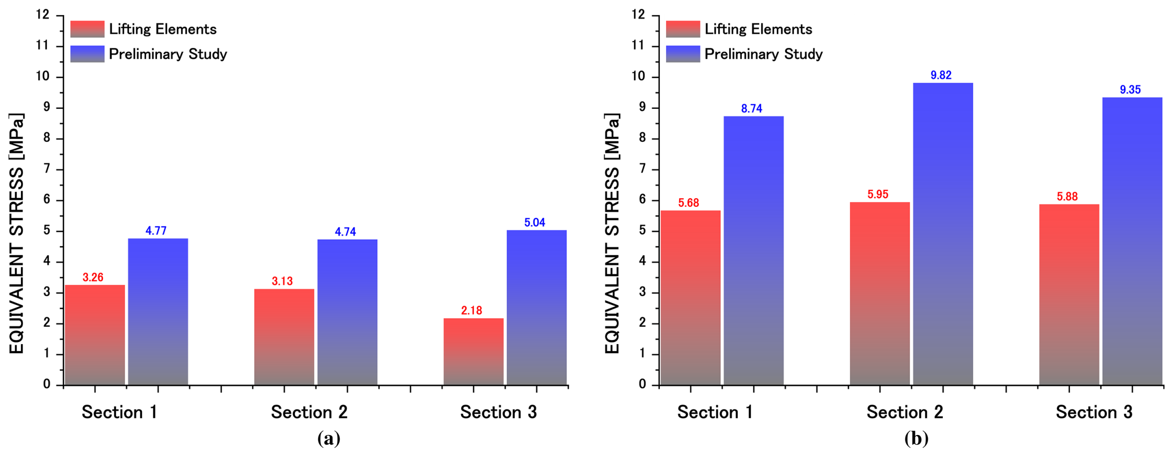

Figure 7: Comparative analysis of maximum stress on GFRP shell. The chart shows the maximum stress before (preliminary study [1]) and after (with lifting system) for both vertical (**a**) and horizontal lifts (**b**).

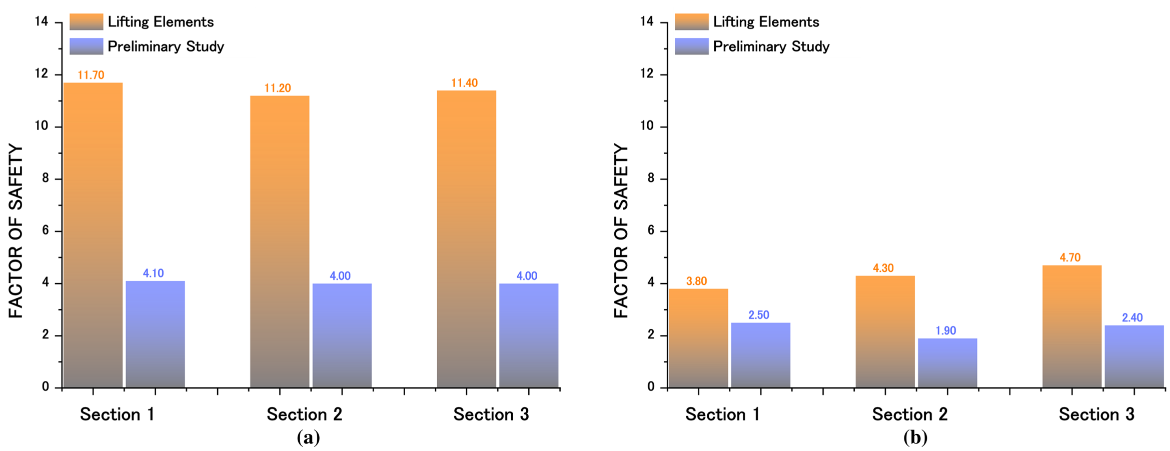

Figure 8: Comparative analysis of minimum factor of safety (FoS) on GFRP shell. The chart shows the minimum FoS before (preliminary study [1]) and after (with lifting system) for both vertical (**a**) and horizontal lifts (**b**).

The structural adequacy of the steel lifting assembly was verified against the requirements of ASME BTH-1 (Design of Below-the-Hook Lifting Devices). For specialized lifting equipment operated under Design Category B service conditions, the standard mandates a minimum design factor of 3.00 against the yield strength of the material. As detailed in the stress distribution maps (Figs. 5b and 6b), the optimized 32 mm steel components exhibit a maximum equivalent stress well below the yield limit of the ASME A36 steel, resulting in a minimum Factor of Safety of 5. This margin significantly surpasses the minimum thresholds established by ASME BTH-1, ensuring that the reinforcement system can accommodate unexpected dynamic load factors or minor eccentricities in the center of gravity without compromising structural integrity. By adhering to these conservative design principles, the maintenance system provides a high degree of reliability for the handling of large-scale, high-value composite assets in variable field environments.

4 Discussion

This study employs established FEA computational analysis to design and validate a novel solution to an unsolved industrial problem [4]. The work serves as a high-impact engineering case study and a methodological blueprint for the structural assessment and retrofitting of aging composite assets. The resulting designed bolt-on steel hoisting system successfully mitigates the critical stress concentrations identified in our prior work [4]. The 31%–35% reduction in maximum stress on the GFRP shell and the corresponding average 286% increase in the factor of safety (FoS) effectively transform an unviable, high-risk lift into a safe, industrially feasible engineering operation. This work is a direct answer to the call for mitigation strategies and careful design of hoisting elements that our baseline study concluded was necessary [4].

4.1 Load Transfer Mechanism and Damage Tolerance of the Proposed System

The primary success of the design lies in its ability to solve the fundamental problem of bolted composite joints: high localized stress [34]. Our baseline study [4] showed stresses concentrated at the bolt holes, a finding consistent with literature that highlights the brittle failure behavior of GFRP in tension and shear [34]. The steel flange system acts as a rigid load-spreader, effectively transferring the load away from the vulnerable composite bolt holes and preventing the local crushing and buckling phenomena common in such joints [50]. By rigidifying the flange, our system prevents the initiation of matrix cracking and delamination, which are known precursors to catastrophic failure [35,37,38]. The design effectively addresses the known failure mechanisms predicted by progressive damage models for bolted connections [53,54]. To quantitatively support this, the Hashin failure criterion was examined at the level of individual damage modes. In the most critical loading scenario (horizontal lift), the peak index for matrix tension (H_{mt}) was found to be 0.26, while the matrix compression index (H_{mc}) remained below 0.15. Since damage initiation in the GFRP is only predicted when any mode index reaches a value of 1.0, these results demonstrate a significant margin against the formation of micro-cracks. This behavior confirms that the lifting system functions as an effective load-spreader, maintaining the interlaminar shear and transverse tensile stresses well below the levels required for matrix degradation [46]. Furthermore, the use of this reinforced assembly effectively addresses the complex failure mechanisms typically predicted by progressive damage models. The results demonstrate that the proposed system achieves a stable global stiffness and reliable load transfer, ensuring that concentrated lifting forces do not exceed the laminate's interlaminar capacity [45]. This reinforces the damage tolerance design philosophy, ensuring the GFRP mantle remains structurally pristine throughout the maintenance maneuver.

Although the Hashin failure criterion used in this study evaluates the onset of damage rather than ultimate failure, the proposed lifting system was designed following a damage tolerance philosophy. The steel blind flange and stiffeners act as the primary load path during lifting operations, significantly reducing the structural demand on the GFRP flange and shell. Therefore, even if localized cracks in the matrix or interlaminar damage in the composite were to initiate due to material aging or manufacturing variability, such damage would not compromise the overall integrity of the system. Stress levels in the GFRP are kept well below those associated with unstable damage propagation or delamination growth. Furthermore, hoisting operations are infrequent maintenance events rather than cyclic service conditions, which inherently limits the possibility of cumulative fatigue damage. This design approach ensures robust structural performance beyond the onset of initial damage and improves the long-term reliability of existing GFRP towers during repeated maintenance operations. Future work involving progressive damage modeling and experimental validation will further quantify the residual strength and long-term performance under sustained maintenance cycles.

Compared to flange reinforcement strategies commonly reported in the literature, such as bonded composite patches, external collars, or clamping systems, the magnitude of the safety margin improvement observed in this study is particularly noteworthy. The literature addressing experimental studies on repairs with bonded patches and externally applied reinforcements typically reports moderate reductions in stress intensity or concentration (<10%) and corresponding increases in fatigue life under service loads [60–62]. While direct numerical equivalence is not possible due to different geometries, load cases, and performance metrics, the average increase of approximately 286% in minimum safety force obtained here for lift-induced load cases substantially exceeds the typical service-oriented improvements associated with adhesive or collar solutions. This contrast highlights the practical advantage of a reversible, bolt-on design specifically conceived to redirect extraordinary lifting loads away from the composite wing.

4.2 Strain Compatibility and Edge Effects at the Steel–FRP Interface

The introduction of a 32 mm thick steel blind flange inevitably increases local structural stiffness. However, the proposed design avoids the formation of harmful hard spots at the steel-GFRP interface by distributing the load transfer through multiple bolted connections and half-moon stiffeners. This arrangement ensures deformation compatibility between the robust steel components and the more compliant GFRP shell. Finite element results indicate smooth deformation continuity throughout the reinforced region, with no abrupt gradients or secondary localized bending at the steel flange boundary. Stress distributions and Hashin failure indices further confirm that no secondary stress concentrations are induced in the adjacent GFRP mantle, even in transitional lifting configurations (angles of 22.5° to 67.5°) where load paths change progressively. Specifically, peak stresses at these boundaries remained below 5.69 MPa, yielding safety factors above 5.60. This behavior demonstrates that the reinforcement functions as a distributed load-transfer system rather than a rigid restraint, thereby successfully mitigating edge effects and preserving the structural integrity of the composite shell.

4.3 Dynamic Amplification Effects during Lifting Operations

The lifting analyses presented here were performed under a quasi-static assumption, applying a nominal lifting load of 50,000 N, representative of controlled lifting operations. In practice, the dynamic effects resulting from acceleration, deceleration, and limited oscillation are commonly incorporated using dynamic amplification factors (DAF) per established standards such as ASME BTH-1. According to ASME BTH-1 Design Category B, which applies to lifting devices with non-precise handling, a typical DAF ranges from 1.1 to 1.3, with a minimum required safety factor of 3.0 on nominal strength. To account for these effects, the proposed system was subjected to a 70,000 N Design Verification Load during the optimization phase, representing a conservative DAF of 1.4. Even at this elevated load, the steel components maintained structural integrity with an FoS of 1.62, while the Hashin failure indices for the GFRP laminate remained significantly below unity. When the reported static FoS of 5.04 for the steel assembly is scaled by a standard DAF of 1.25, the resulting operational FoS of 4.03 still comfortably exceeds the regulatory requirements. This confirms that the proposed lifting system maintains adequate safety margins when considering the realistic effects of dynamic amplification.

4.4 Practical Feasibility and Long-Term Durability

Although the proposed lifting system is described as non-invasive, its implementation in existing industrial towers requires standard pre-installation inspections. In this context, non-invasiveness refers specifically to the absence of permanent structural modifications to the GFRP laminate, such as additional drilling, bonding, or removal of material. The fully bolted configuration ensures reversibility and preserves the original structural integrity of the tower sections. Practical aspects of installation, such as internal access under the flange, available clearance with respect to packing elements or coatings, and the local condition of the composite material, must be evaluated on a case-by-case basis for older assets. These evaluations are consistent with standard industrial maintenance practices and do not limit the applicability of the proposed solution.

Regarding long-term durability, potential galvanic corrosion at steel-GFRP interfaces in humid or chemically aggressive environments is a recognized concern for hybrid structural components. While GFRP is inherently an electrical insulator, electrochemical interactions can occur at metal-composite interfaces when moisture films act as electrolytes. Previous studies have shown that corrosion risks in steel-GFRP hybrid systems can be effectively mitigated by using dielectric insulation layers and protective epoxy coatings on the steel components, as well as by selecting corrosion-resistant fasteners (e.g., galvanized or stainless steel hardware), which have been shown to significantly reduce galvanic attack in accelerated environmental exposures [13,57,58]. These established measures ensure that the introduction of steel lifting elements does not compromise the corrosion resistance or long-term durability of the composite structure during its remaining service life.

Various mitigation techniques at the joint level, such as adhesive filling, modifying bolt geometry, or using elliptical perforations has been reported [40,42,43]. The efficacy of joint-level modifications proposed by Li et al. [36] verified that adhesive filling and optimized hole shapes effectively mitigate local stress concentrations. While scientifically robust, these methods pose practical challenges for *in-situ* maintenance, our solution provides a macro-level, non-invasive system that requires no permanent modification or chemical bonding to the composite tower itself. This distinction is crucial: this bolt-on approach is critical for aging assets where surface contamination may compromise adhesives [36], the original manufacturing quality is unknown [45], and long-term durability is a primary concern [20]. The design's validation under transitional angles (22.5°–67.5°) also represents a significant contribution, as it addresses complex, multi-axial loads not captured in standard joint analyses [27].

The practical contribution of this paper is a industry-ready, validated blueprint for the safe maintenance of existing industrial GFRP assets [24,25]. This is a tangible solution for the service-life challenges of composite structures [17], moving beyond simple structural comparisons [58] to a hybrid, real-world application. Theoretically, our work demonstrates a successful application of composite-steel hybrid design, where the steel's isotropy and stiffness are used to protect the composite's anisotropic vulnerabilities. This validated FEA model serves as a framework for future progressive damage analyses and can be used to assess the remaining service life of similar structures [26,30].

4.5 Limitations and Future Work

The primary limitation of this study is the absence of full-scale experimental validation; therefore, the findings constitute a high-fidelity computational baseline. Given the operational constraints of the industrial tower, the FEA relies on established standards (e.g., ASME RTP-1) and a bonded-contact assumption for the 48-bolt interface—a methodology previously validated in Mariqueo and Tuninetti [4]. While this approach effectively predicts global stiffness and stress paths, it does not explicitly capture dynamic load amplification or potential bolt slip. In addition, the finite element analyses presented here use the properties of FRP material derived from the ASME RTP-1 standard, which represents nominal values for newly manufactured composite structures. It is recognized that FRP towers in service may experience material degradation over time due to environmental exposure, including UV radiation, chemical attack, and moisture ingress, which could reduce their stiffness and strength. This degradation could increase the vulnerability of unreinforced composite flanges during lifting operations. However, the proposed bolted steel lifting system is specifically designed to transfer most of the lifting-induced loads away from the FRP components, thereby reducing the sensitivity of the system to variations in composite material properties [63]. Accordingly, it is expected that the effectiveness of the proposed solution will be maintained, and even improved, for aged structures.

Future work should focus on controlled experimental testing of representative or scaled GFRP shell segments. To provide a comprehensive validation, future setups will employ a combination of traditional strain gauges and full-field Digital Image Correlation (DIC). This integrated approach will allow for high-resolution mapping of strain gradients around the reinforcement pattern, enabling the empirical validation of the predicted Hashin failure indices and the identification of localized damage initiation. Such testing will provide the final level of confidence required to transition this reinforcement system into broad field implementation for aging composite infrastructure.

5 Conclusions

This study presented the design and comprehensive FEA validation of a novel, bolt-on steel hoisting system to address the significant structural risks associated with lifting GFRP absorption towers. The new design successfully transferred loads from the vulnerable composite flanges to the robust steel components, resulting in a 31% reduction in maximum stress on the GFRP shell in vertical lifts and a 35% reduction during the more critical horizontal lifts. This stress reduction improved structural integrity, increasing the minimum safety factor from a critical 1.9 to a safe 3.8 in the horizontal case and from 4.1 to 11.7 in the vertical case (an average increase of 286%). The steel components were validated with a minimum FoS of 5.04, and the ASME A307 bolts showed an FoS over 40. These safety margins comfortably exceed the minimum requirements commonly prescribed by ASME BTH-1 for under-the-hook lifting devices, which typically specify safety factors in the order of 3.0 depending on the service classification and load conditions.

The validation presented in this paper applies to specific tower geometry, laminate configuration, material properties, and hoisting load cases investigated. While the proposed bolted system demonstrates clear effectiveness for this configuration, its application to other FRP composite towers would require a similar structural evaluation, adapted to the geometry, laminate stack-up, and corresponding operational loading conditions. Nevertheless, the methodology and design approach presented here provide a transferable framework for the evaluation of safe lifting and modernization of comparable composite structures.

Acknowledgement: Not applicable.

Funding Statement: The authors received no specific funding for this study.

Author Contributions: Matías Mariqueo: Conceptualization, Methodology, Software, Validation, Formal Analysis, Investigation, Data Curation. Rodrigo Valle: Investigation, Writing—Review & Editing. César Garrido: Visualization, Writing—Review & Editing. Sebastián Andrés Toro: Investigation, Writing—Review & Editing. Víctor Tuninetti: Conceptualization, Methodology, Validation, Resources, Writing—Original Draft, Writing—Review & Editing, Supervision, Project Administration. All authors reviewed and approved the final version of the manuscript.

Availability of Data and Materials: Data available within the article.

Ethics Approval: Not applicable.

Conflicts of Interest: The authors declare no conflicts of interest.

References

1. Hampaiyan Miandowab H, Bidadi J, Saeidi Googarchin H. Influences of freeze, water immersion, and cyclic freeze-thaw environmental conditions on crashworthiness performance of GFRP circular tubes subjected to axial and lateral quasi-static load. Compos Commun. 2025;57(6):102490. doi:10.1016/j.coco.2025.102490.
2. Shahkhosravi NA, Yousefi J, Najafabadi MA, Burvill C, Minak G. Fatigue life reduction of GFRP composites due to delamination associated with the introduction of functional discontinuities. Compos Part B Eng. 2019;163(4):536–47. doi:10.1016/j.compositesb.2019.01.005.
3. Satheesh Raja R, Manisekar K. Experimental and statistical analysis on mechanical properties of nano flyash impregnated GFRP composites using central composite design method. Mater Des. 2016;89:884–92. doi:10.1016/j.matdes.2015.10.043.
4. Tuninetti V, Mariqueo M. Performance of combined woven roving and mat glass-fiber reinforced polymer composites under absorption tower lifting loads. Polymers. 2024;16(20):2937. doi:10.3390/polym16202937.
5. Jiang L, Wang X, Cheng X, Zhou Y, Yi Y. A review of moisture absorption and corrosion resistance performance of FRTP in marine environments. Polym Test. 2025;145(12):108760. doi:10.1016/j.polymertesting.2025.108760.
6. Ascione F, Maselli G, Nesticò A. Sustainable materials selection in industrial construction: a life-cycle based approach to compare the economic and structural performances of glass fibre reinforced polymer (GFRP) and steel. J Clean Prod. 2024;475:143641. doi:10.1016/j.jclepro.2024.143641.
7. Awad YA, El-Fiky AM, Hegazy HM, Hasan MG, Yousef IA, Ebid AM, et al. Measuring and rigidity moduli of GFRP experimentally. Civ Eng J. 2023;9(8):1912–21. doi:10.28991/cej-2023-09-08-07.
8. Farzana M, Haque MM, Sonali SM, Mollah MZI, Amin MA, Khan SA, et al. Thermo-mechanical properties and applications of glass fiber reinforced polymer composites. Mod Concepts Mater Sci. 2023;5(3):1–9. doi:10.33552/mcms.2023.05.000614.
9. Meddour M, Si Salem A, Ait Taleb S. Bending behavior of new composited sandwich panels with GFRP waste based-core and PVC facesheets: experimental design, modeling and optimization. Constr Build Mater. 2024;426:136117. doi:10.1016/j.conbuildmat.2024.136117.
10. Ali Sebeay T, Ahmed A. Numerical investigation into GFRP composite pipes under hydrostatic internal pressure. Polymers. 2023;15(5):1110. doi:10.3390/polym15051110.
11. Hassan MK, Redhwi AMN, Mohamed AF, Backar AH, Abdellah MY. Investigation of erosion/corrosion behavior of GRP under harsh operating conditions. Polymers. 2022;14(24):5388. doi:10.3390/polym14245388.
12. Ebrahimzadeh S, Manalo A, Alajarmeh O, Yang X, Benmokrane B, Sorbello CD, et al. Structural performance of the GFRP-reinforced precast concrete no-gap boat ramp plank. Eng Struct. 2025;335(1):120289. doi:10.1016/j.engstruct.2025.120289.
13. Alabtah FG, Mahdi E, Khraisheh M. External corrosion behavior of steel/GFRP composite pipes in harsh conditions. Materials. 2021;14(21):6501. doi:10.3390/ma14216501.
14. Elkafrawy M, Gowrishankar P, Aswad NG, Alashkar A, Khalil A, AlHamaydeh M, et al. GFRP-reinforced concrete columns: state-of-the-art, behavior, and research needs. Buildings. 2024;14(10):3131. doi:10.3390/buildings14103131.
15. Oropesa Y, Araya N, Oñate A, Maril M, Sauceda S, Vargas-Silva G, et al. Composite materials for lightweight and high-performance aerospace structures. Proc Inst Mech Eng Part L J Mater Des Appl. 2026. doi:10.1177/14644207261429085.
16. Mincigrucci L, Civera M, Lenticchia E, Ceravolo R, Rosano M, Russo S. Comparative structural analysis of GFRP, reinforced concrete, and steel frames under seismic loads. Materials. 2023;16(14):4908. doi:10.3390/ma16144908.
17. Zhao M, Dong Y, Guo H. Comparative life cycle assessment of composite structures incorporating uncertainty and global sensitivity analysis. Eng Struct. 2021;242:112394. doi:10.1016/j.engstruct.2021.112394.

18. Frigione M, Lettieri M. Durability issues and challenges for material advancements in FRP employed in the construction industry. Polymers. 2018;10(3):247. doi:10.3390/polym10030247.
19. Hizam RM, Manalo AC, Karunasena W, Bai Y. Behaviour of pultruded GFRP truss system connected using through-bolt with mechanical insert. Compos Part B Eng. 2019;168(6):44–57. doi:10.1016/j.compositesb.2018.12.052.
20. Abu Bakar MS, Mohamad D, Ishak ZAM, Yusof ZM, Salwi N. Durability control of moisture degradation in GFRP cross arm transmission line towers. AIP Conf Proc. 2018;2031(1):020027. doi:10.1063/1.5066983.
21. Saeedi A, Motavalli M, Shahverdi M. Recent advancements in the applications of fiber-reinforced polymer structures in railway industry—a review. Polym Compos. 2024;45(1):77–97. doi:10.1002/pc.27817.
22. Richard D, Hong T, Hastak M, Mirmiran A, Salem O. Life-cycle performance model for composites in construction. Compos Part B Eng. 2007;38(2):236–46. doi:10.1016/j.compositesb.2006.04.001.
23. Zhu Y, Fascetti A, Feo L, Mosallam AS, Penna R. Experimental and numerical characterization of pultruded GFRP structural elements with stiffened Web-Flange junctions. Compos Struct. 2023;303(4):116383. doi:10.1016/j.compstruct.2022.116383.
24. Syamsir A, Ean L-W, Asyraf M, Supian A, Madenci E, Özkılıç Y, et al. Recent advances of GFRP composite cross arms in energy transmission tower: a short review on design improvements and mechanical properties. Materials. 2023;16(7):2778. doi:10.3390/ma16072778.
25. Lagos F, Menacer B, Salas A, Narayan S, Medina C, Valle R, et al. Recent advances in the analysis of functional and structural polymer composites for wind turbines. Polymers. 2025;17(17):2339. doi:10.3390/polym17172339.
26. Gao G, An L, Giannopoulos IK, Han N, Ge E, Hu G. Progressive damage numerical modelling and simulation of aircraft composite bolted joints bearing response. Materials. 2020;13(24):5606. doi:10.3390/ma13245606.
27. Montagne B, Lachaud F, Paroissien E, Martini D, Congourdeau F. Failure analysis of single lap composite laminate bolted joints: comparison of experimental and numerical tests. Compos Struct. 2020;238:111949. doi:10.1016/j.compstruct.2020.111949.
28. Valdivia I, Canales C, Tuninetti V, Flores P, Medina C. Numerical prediction of failure in unidirectional fiber reinforced composite. Int J Appl Mechanics. 2021;13(6):2150073. doi:10.1142/s1758825121500733.
29. Tuninetti V, Medina C, Salas A, Valdivia I, Fernández E, Meléndrez M, et al. Fiber-reinforced composite materials: characterization and computational predictions of mechanical performance. Cham, Switzerland: Springer Nature Switzerland; 2023.
30. Nerilli F, Tarquini L, Marino M, Vairo G. Numerical modeling of failure modes in bolted composite laminates. AIP Conf Proc. 2015;1648(1):570019. doi:10.1063/1.4912805.
31. Wang X, Wang Y, Ji Y, Hu H, Cao D, Zheng K, et al. Modeling progressive damage and failure of single-lap thin-ply-laminated composite-bolted joint using LaRC failure criterion. Materials. 2022;15(22):8123. doi:10.3390/ma15228123.
32. Wang M, Hang X. Finite element analysis of residual stress distribution patterns of prestressed composites considering interphases. Materials. 2023;16(4):1345. doi:10.3390/ma16041345.
33. Weisova M, Kotrasova K, Kvocak V. The numerical study of the reinforcement layer orientation effect on the behaviour of laminated plates. E3S Web Conf. 2024;550(6):01034. doi:10.1051/e3sconf/202455001034.
34. Rahman A, Boem I, Gattesco N. Numerical study on the performance and failure modes of bolted connections in pultruded-fibre-reinforced polymer (PFRP) profiles. J Compos Sci. 2025;9(9):492. doi:10.3390/jcs9090492.
35. Garoz D, Hajikazemi M, Dinh TD, Van Paepegem W. Mesoscale finite element analysis of cracked composite laminates under out-of-plane loads using 3D periodic boundary conditions. Compos Struct. 2020;235:111699. doi:10.1016/j.compstruct.2019.111699.
36. Li D, Wu F, Cai Z, Almutairi AD, Zhou J, Dai Y. Stress concentration in glass fiber reinforced polymer plates induced by central circular holes and bolted connections. Case Stud Constr Mater. 2025;23(9):e05356. doi:10.1016/j.cscm.2025.e05356.
37. Khan A, Azad MM, Sohail M, Kim HS. A review of physics-based models in prognostics and health management of laminated composite structures. Int J Precis Eng Manuf Green Technol. 2023;10(6):1615–35. doi:10.1007/s40684-023-00509-4.

38. Taherzadeh-Fard A, Cornejo A, Jiménez S, Barbu LG. Numerical analysis of damage in composites: from intra-layer to delamination and data-assisted methods. Mathematics. 2025;13(10):1578. doi:10.3390/math13101578.
39. Abdel-Monsef S, Elsisi A, Maaly H, El-Hosseiny O. Performance of pultruded FRP beam-column connections under different design parameters. J Compos Sci. 2025;9(9):487. doi:10.3390/jcs9090487.
40. Dai Y, Chen J, Yu C, Almutairi AD, Yuan Y. Comparative analysis of strength improvement techniques in perforated glass fiber reinforced polymer plates: adhesive filling, bolt reinforcement, and elliptical perforation design. Materials. 2025;18(18):4290. doi:10.3390/ma18184290.
41. Toubia EA, Alomari A, Morgan AB, Klosterman D. Influence of heat damage on the bolted double lap joint strength of pultruded E-glass/polyester composites. Thin Walled Struct. 2021;163(6):107764. doi:10.1016/j.tws.2021.107764.
42. Hu B, Chen X, Deng F, Sun X. Evaluation of failure criteria for residual tensile strength of composite laminates with circular holes. Vib Proced. 2023;49:212–9. doi:10.21595/vp.2023.23348.
43. Orun AE, Salamci E, Coker D. Investigation of reinforcement around the lightening hole in composite plates under tension and shear loads. Mech Compos Mater. 2024;60(1):183–98. doi:10.1007/s11029-024-10182-6.
44. Lobanov D, Yankin A, Mullahmetov M, Chebotareva E, Melnikova V. The analysis of stress raisers affecting the GFRP strength at quasi-static and cyclic loads by the theory of critical distances, digital image correlation, and acoustic emission. Polymers. 2023;15(9):2087. doi:10.3390/polym15092087.
45. Qi Z, Liang G, Dai Y, Qiu J, Hao H. The effects of countersink depth on fatigue performance of CFRP joint. Int J Adv Manuf Technol. 2023;128(9):4397–412. doi:10.1007/s00170-023-12130-5.
46. Gopalan R, Narayanan P. Experimental and numerical evaluation of pultruded GFRP double-lap joints with different mechanical fasteners. Results Eng. 2023;18:101035. doi:10.1016/j.rineng.2023.101035.
47. Liang M, Wang X, Yuan X, Correia JR, Wu Z. Behaviors and load distribution of sleeved bolted joints between pultruded FRP box profiles with multi-directional fiber layups. Compos Struct. 2025;373(2):119673. doi:10.1016/j.compstruct.2025.119673.
48. He X. A review of finite element analysis of adhesively bonded joints. Int J Adhes Adhes. 2011;31(4):248–64. doi:10.1016/j.ijadhadh.2011.01.006.
49. Magliaro J, Altenhof W, Alpas AT. A review of advanced materials, structures and deformation modes for adaptive energy dissipation and structural crashworthiness. Thin Walled Struct. 2022;180:109808. doi:10.1016/j.tws.2022.109808.
50. Tao X, Cao S, Zhang L. Elastic stability of perforated plates strengthened with FRP under uniaxial compression. Appl Sci. 2017;7(11):1188. doi:10.3390/app7111188.
51. Raghunathan MD, Senthil R, Palani GS. On the tensile capacity of single-bolted connections between GFRP angles and gusset plates-testing and modelling. KSCE J Civ Eng. 2017;21(6):2259–72. doi:10.1007/s12205-016-1102-4.
52. Chen C, Fang H, Han J, Qi Y. Structural performance evaluation of pultruded GFRP composite space truss: experimental study and numerical simulation. Case Stud Constr Mater. 2022;17:e01551. doi:10.1016/j.cscm.2022.e01551.
53. Luo B, Xue L, Wang Q, Zou P. Mechanistic study of failure in CFRP hybrid bonded-bolted interference connection structures under tensile loading. Materials. 2024;17(9):2117. doi:10.3390/ma17092117.
54. Li X, Xie Z, Zhao W, Zhang Y, Gong Y, Hu N. Failure prediction of irregular arranged multi-bolt composite repair based on finite fracture mechanics model. Eng Fract Mech. 2021;242:107456. doi:10.1016/j.engfracmech.2020.107456.
55. Ahmed MS, Sennah K, Afefy HM. Fatigue and ultimate strength evaluation of GFRP-reinforced, laterally-restrained, full-depth precast deck panels with developed UHPFRC-filled transverse closure strips. Appl Sci. 2024;14(19):8806. doi:10.3390/app14198806.
56. Sümer Y, Öztemel M. Investigation of the effect of GFRP reinforcement bars on the flexural strength of reinforced concrete beams using the finite element method. Fibers. 2025;13(9):125. doi:10.3390/fib13090125.
57. Manoj Prabhakar M, Rajini N, Ayrilmis N, Mayandi K, Siengchin S, Senthilkumar K, et al. An overview of burst, buckling, durability and corrosion analysis of lightweight FRP composite pipes and their applicability. Compos Struct. 2019;230:111419. doi:10.1016/j.compstruct.2019.111419.

58. Alshurafa S, Polyzois D. Design recommendations and comparative study of FRP and steel guyed towers. Eng Sci Technol Int J. 2018;21(5):807–14. doi:10.1016/j.jestch.2018.06.014.
59. Tanlak N, Sonmez FO, Talay E. Detailed and simplified models of bolted joints under impact loading. J Strain Anal Eng Des. 2011;46(3):213–25. doi:10.1177/0309324710396997.
60. Aabid A, Hrairi M, Ali JSM, Ali Sebaey T. A review on reductions in the stress-intensity factor of cracked plates using bonded composite patches. Materials. 2022;15(9):3086. doi:10.3390/ma15093086.
61. Borrie D, Al-Saadi S, Zhao XL, Singh Raman RK, Bai Y. Bonded CFRP/steel systems, remedies of bond degradation and behaviour of CFRP repaired steel: an overview. Polymers. 2021;13(9):1533. doi:10.3390/polym13091533.
62. Xing R, Wang F, Yang Y, Li G. Optimization of composite material repair patch shape based on strength analysis. Appl Sci. 2024;14(11):4397. doi:10.3390/app14114397.
63. Dziomdziora P, Smarzewski P. Reinforced concrete beams with FRP and hybrid steel-FRP composite bars: load-deflection response, failure mechanisms, and design implications. Materials. 2025;18(18):4381. doi:10.3390/ma18184381.